Institute for Advanced Technology
The University of Texas at Austin

IAT

Electrical and Thermal Effects of Rail Cladding in a Full-Scale Launcher

S. Levinson and J. Parker

Institute for Advanced Technology
The University of Texas at Austin

April 1998

IAT.R 0168

REPORT DOCUMENTATION PAGE

Form Approved
OMB NO. 0704-0188

1. AGENCY USE ONLY (Leave blank)	2. REPORT DATE	3. REPORT TYPE AND DATES COVERED
	April 1998	Technical Report July 1997 - April 1998

4. TITLE AND SUBTITLE

Electrical and Thermal Effects of Rail Cladding in a Full-Scale Launcher

5. FUNDING NUMBERS

Contract # DAAA21-93-C-0101

6. AUTHOR(S)

S. Levinson and J. Parker

7. PERFORMING ORGANIZATION NAME(S) AND ADDRESS(ES)

Institute for Advanced Technology
The University of Texas at Austin
4030-2 W. Braker Lane, #200
Austin, TX 78759

8. PERFORMING ORGANIZATION REPORT NUMBER

IAT.R 0168

9. SPONSORING / MONITORING AGENCY NAME(S) AND ADDRESS(ES)

U.S. Army Research Laboratory
ATTN: AMSRL-WT-T
Aberdeen Proving Ground, MD 21005-5066

10. SPONSORING / MONITORING AGENCY REPORT NUMBER

11. SUPPLEMENTARY NOTES

The view, opinions and/or findings contained in this report are those of the author(s) and should not be considered as an official Department of the Army position, policy, or decision, unless so designated by other documentation.

12a. DISTRIBUTION / AVAILABILITY STATEMENT

Approved for public release; distribution unlimited.

12b. DISTRIBUTION CODE

A

13. ABSTRACT *(Maximum 200 words)*

A previous paper reported the computational simulation of a resistive rail cladding in a 40 mm bore railgun [1]. In that study, it was found that a 1 mm thick resistive rail cladding (10 mW•cm or 50 mW•cm) on a copper rail (2 mW•cm) resulted in an additional electrical loss equal to about 5% of the muzzle energy, corresponding to a reduction in the overall launch efficiency of less than 1%. This report extends the previous cladding study to a 90 mm bore, near full-scale railgun. The base rail material resistivity has been increased to 4.5 W-cm, typical of the low density alloys that may be needed in a practical launcher. It is found that a 1 mm resistive cladding in the near full-scale launcher has only one half the impact on efficiency calculated previously for a 40 mm bore. For example, a 100 mW•cm cladding results in an additional electrical loss equal to 2.4% of the muzzle kinetic energy, resulting in reduction in overall launcher efficiency of less than 1/2%.

14. SUBJECT TERMS

cladding, finite element analysis (FEA), loss, railgun

15. NUMBER OF PAGES

22

16. PRICE CODE

17. SECURITY CLASSIFICATION OF REPORT	18. SECURITY CLASSIFICATION OF THIS PAGE	19. SECURITY CLASSIFICATION OF ABSTRACT	20. LIMITATION OF ABSTRACT
Unclassified	Unclassified	Unclassified	UL

Table of Contents

List of Figures

List of Tables

Electrical and Thermal Effects of Rail Cladding in a Full-Scale Launcher

Scott Levinson and Jerry Parker

Abstract

A previous paper reported the computational simulation of a resistive rail cladding in a 40 mm bore railgun [1]. In that study, it was found that a 1 mm thick resistive rail cladding (10 μΩ•cm or 50 μΩ•cm) on a copper rail (2 μΩ•cm) resulted in an additional electrical loss equal to about 5% of the muzzle energy, corresponding to a reduction in the overall launch efficiency of less than 1%. This report extends the previous cladding study to a 90 mm bore, near full-scale railgun. The base rail material resistivity has been increased to 4.5 Ω–cm, typical of the low density alloys that may be needed in a practical launcher. It is found that a 1 mm resistive cladding in the near full-scale launcher has only one half the impact on efficiency calculated previously for a 40 mm bore. For example, a 100 μΩ•cm cladding results in an additional electrical loss equal to 2.4% of the muzzle kinetic energy, resulting in reduction in overall launcher efficiency of less than 1/2%.

I. Introduction

The motivation, background and results of a study on the use of a 1 mm resistive cladding on copper rails in a 40 mm bore electric launcher are described in [1], which is attached for reference as an appendix. This report extends that analysis to a 90 mm bore, near full-scale launcher. The same approach is used in this study as in [1]: a 2-D analysis is performed using EMAP3D to calculate the distribution of current and temperature behind the armature. A 3-D analysis is performed in the portion of the rail directly under the armature. The cladding (Ohmic) losses calculated in the two analyses are combined to obtain the total loss. An identical calculation is performed without the resistive cladding for comparison. The relative importance of cladding loss is quantified using a figure of merit defined as the difference in ohmic losses with and without rail cladding divided by the kinetic energy of the launch package.

The report is organized as follows. Section II describes the 90 mm launcher modeled with EMAP3D. In Section III, the results of a 2-D analysis of losses behind the armature are described. Section IV then treats the 3-D analysis of losses in the cladding in the vicinity of a moving armature. Conclusions based on these analyses are given in Section V.

II. Model Of Rail Claddings

The full-scale, 90 mm rectangular bore launcher studied in this work consists of a "C" shaped aluminum armature, a pair of rails that are assumed to be a low density alloy material (ρ=4.5 μΩ·cm), and a pair of 1 mm resistive rail claddings. A quarter section of this geometry is shown in Figure 1. Cladding resistivities of 10 μΩ•cm, 50 μΩ•cm, and 100 μΩ•cm are considered. The 40 mm bore launcher described in [1] had similar materials for the armature and for the 1 mm resistive rail claddings, but the rails were modeled as copper base material (ρ=2 μΩ•cm) for comparison with our laboratory launcher.

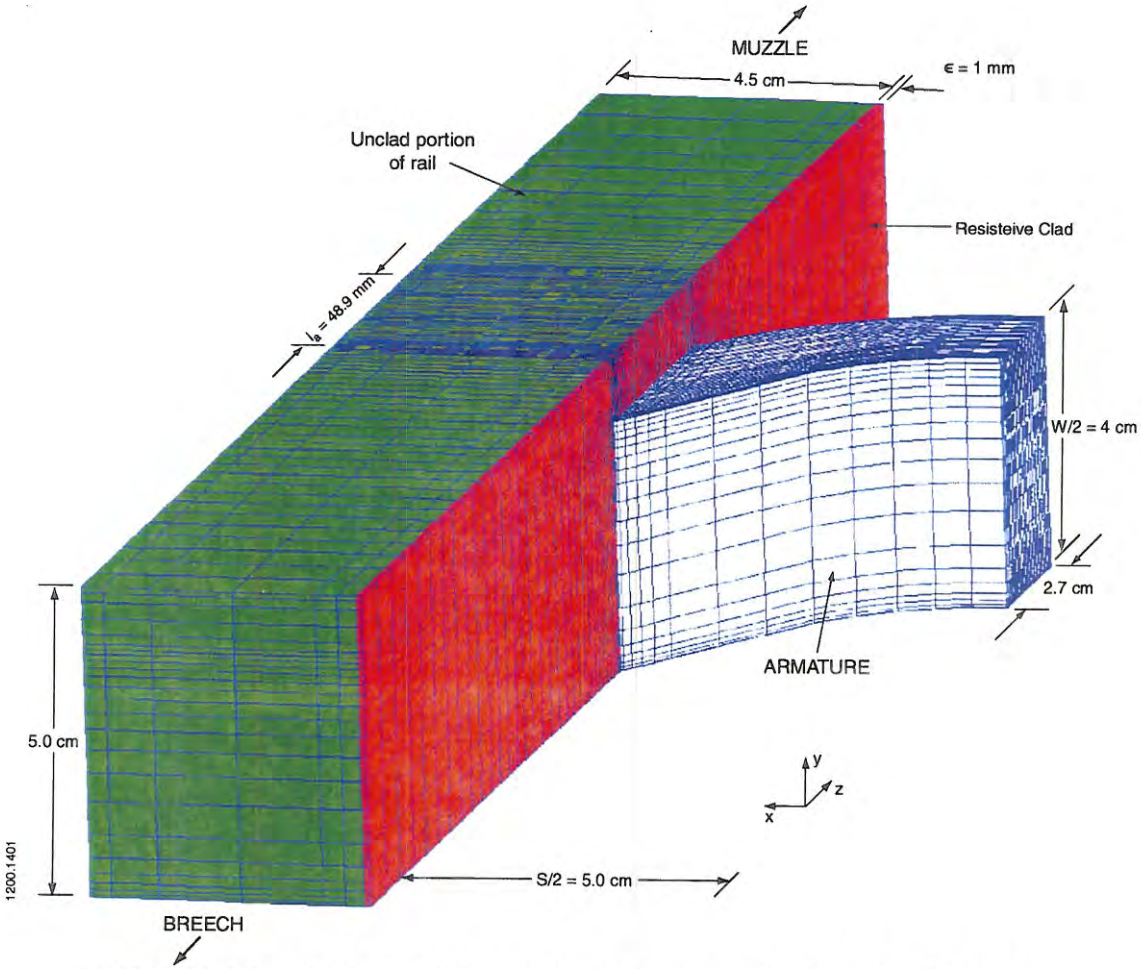

Figure 1. One-quarter model of railgun geometry showing the FE mesh.

The finite element model for the full-scale launcher required 60912 elements and 66500 nodes to satisfactorily model the electro-thermal diffusive behavior of a resistive cladding. The following parameters are assumed in the calculations: The railgun material properties, electrical resistivity and specific heat used in the simulations are given in Tables 1 and 2.

Table 1: Material Resistivities for 90 mm bore launcher

Component	Electrical Resistivity (μΩ•cm)
Aluminum Armature	6.67
Rail	4.5
Cladding	4.5, 10, 50, & 100

Table 2: Specific heat for materials in 90 mm bore launcher

Component	Temperature (°K)	Specific Heat C_p (MJ m^{-3} $°K^{-1}$)
Rail & Cladding	298	3.39
Rail & Cladding	350	3.44
Rail & Cladding	1250	4.28
Aluminum	All	2.749

Model parameters such as launch package mass and acceleration are chosen to approximate the characteristics of a tank application.

- total launch mass — $M_T = 6.4$ kg
- total launch kinetic energy — $E_T = 2 \cdot 10^7$ J
- payload fraction — pf = 50 %
- barrel length — $l_b = 7$ m
- piezometric efficiency — $e_f = 75\%$
- inductive gradient — $L' = 5 \cdot 10^{-7}$ H/m
- peak base pressure — $P_p = 4.76 \cdot 10^8$ Pa (70 ksi)
- armature's axial contact length — $l_a = 48.9$ mm

To simplify modeling, the detailed current waveform of a real launcher is replaced by a constant current. The parameters of this equivalent constant current launcher are given below. This approximation will result in a small underestimation of the overall losses but the relative effect of the cladding will be accurately simulated.

• Length of Launcher	$L_o = e_f \cdot l_b$	$= 5.25$ m
• Force	$F_p = E_T / L_o$	$= 3.81 \cdot 10^6$ N
• Bore Area	F_p / P_p $= W \cdot S$	$= 8 \cdot 10^{-3}$ m^2 $= 80$ mm $\cdot 100$ mm
• Armature Contact Area	$= W \cdot l_a$	$= 80$ mm $\cdot$ 48.9 mm
• Launch Current	$I = \sqrt{\frac{2F_p}{L'}}$	$= 3.9 \cdot 10^6$ A
• Acceleration	$a = F_p / M_T$	$= 5.95 \cdot 10^5$ m/s^2
• Exit Velocity	$v_e = \sqrt{2 \cdot E_T / M_T}$	$= 2500$ m/s
• Exit Time	$t_e = v_e / a$	$= 4.2$ ms

III. 2-D Loss Component

We first consider the component of electrical loss at large distances behind the armature, where the current density in the rail and cladding is essentially $J=J_z$, unaffected by the armature and the diffusive processes are accurately described by equations in two dimensions. As in [1], the 2-D ohmic loss gradients are calculated as a function of time for a constant current flowing axially in the rail with and without cladding. The total 2-D energy loss component is then obtained by integrating the loss gradients over the rail length using the armature position versus time for a constant acceleration to convert the time dependence of the 2-D solutions to a spatial dependence.

An example of a 2-D simulation of the current density distribution J is shown in Figure 2 for a 4.5 μΩ•cm rail and 100 μΩ•cm cladding at $t_e = 4.2$ ms. Note that the peak current density $J=J_{max}(x,y) = 1.2$ GA/m^2 exists at the top of the rail adjacent to the cladding. Current has diffused rapidly through the cladding and J is a factor of 30 smaller in the 100 μΩ•cm cladding. Figure 3 shows the corresponding temperature distribution for each of four cladding cases resulting from the accumulated ohmic heating at 4.2 ms. Note that the hottest cladding temperature occurs in the low resistivity case (control: 4.5 μΩ•cm), and the cladding temperature decreases as resistivity increases. The temperature in the underlying rail increases with increasing cladding resistivity as current is diverted into the rail.

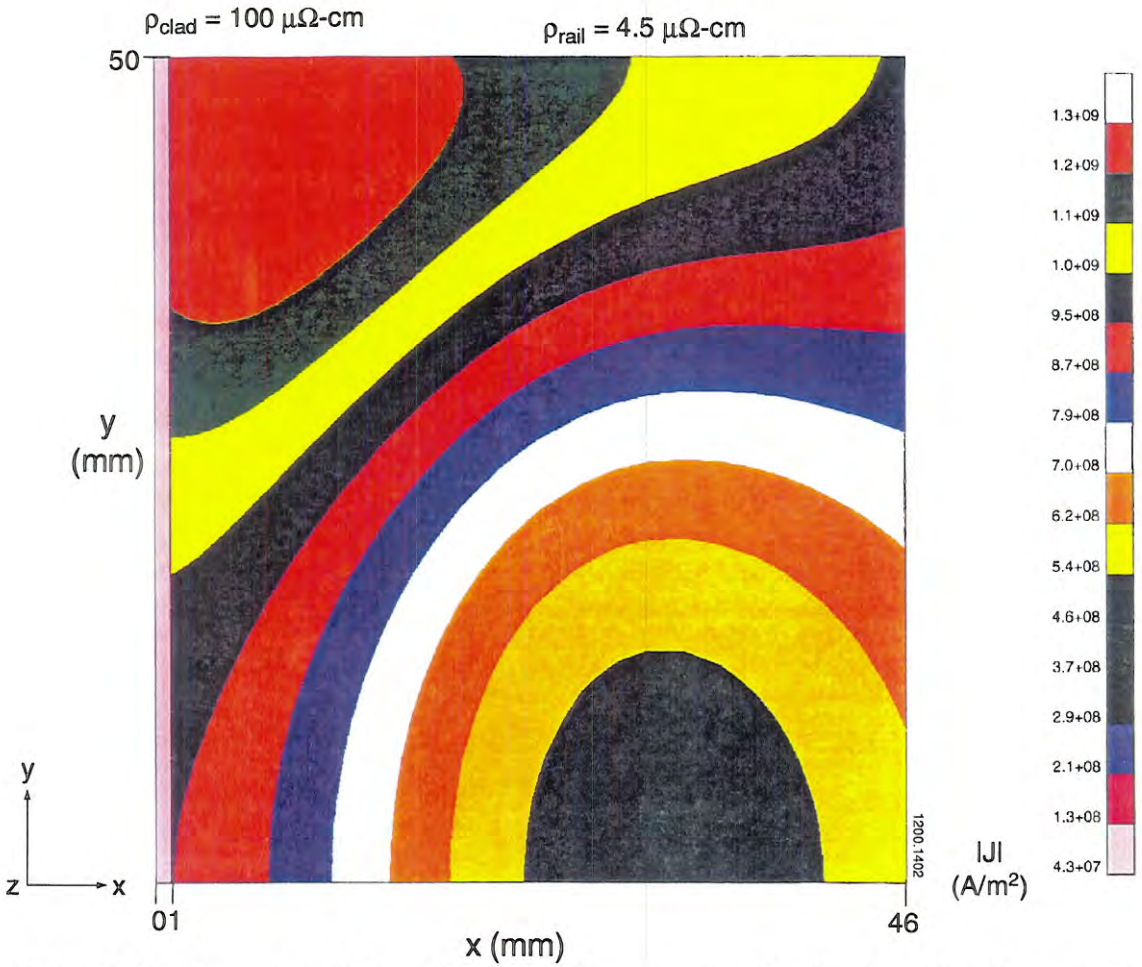

Figure 2. Contour plot of the rail and cladding current distribution |J(x,y)| near the breech at exit time for a rail with 4.5 μΩ•cm resistivity and cladding with 100 μΩ•cm resistivity. 2-D calculation using EMAP3D.

The thermal energy deposited per unit length as a function of time provides a quantitative means for evaluating the relative efficiency of a launcher with a resistive cladding. Figure 4a shows the energy deposited per unit length for each cladding case. Energy deposition is greatest for the control cladding (2.85 Ω kJ/cm at t_e =4.2 ms), and the loss decreases monotonically with cladding resistivity. The 100 μΩ·cm cladding has the smallest loss gradient of the cases evaluated (0.484 kJ/m at t_e =4.2 ms).

Figure 4b shows the total energy dissipated per unit length in rail and cladding combined. This quantity, designated E_2', is greater (as expected) for the resistive claddings although the change is too small to be seen in the plot.

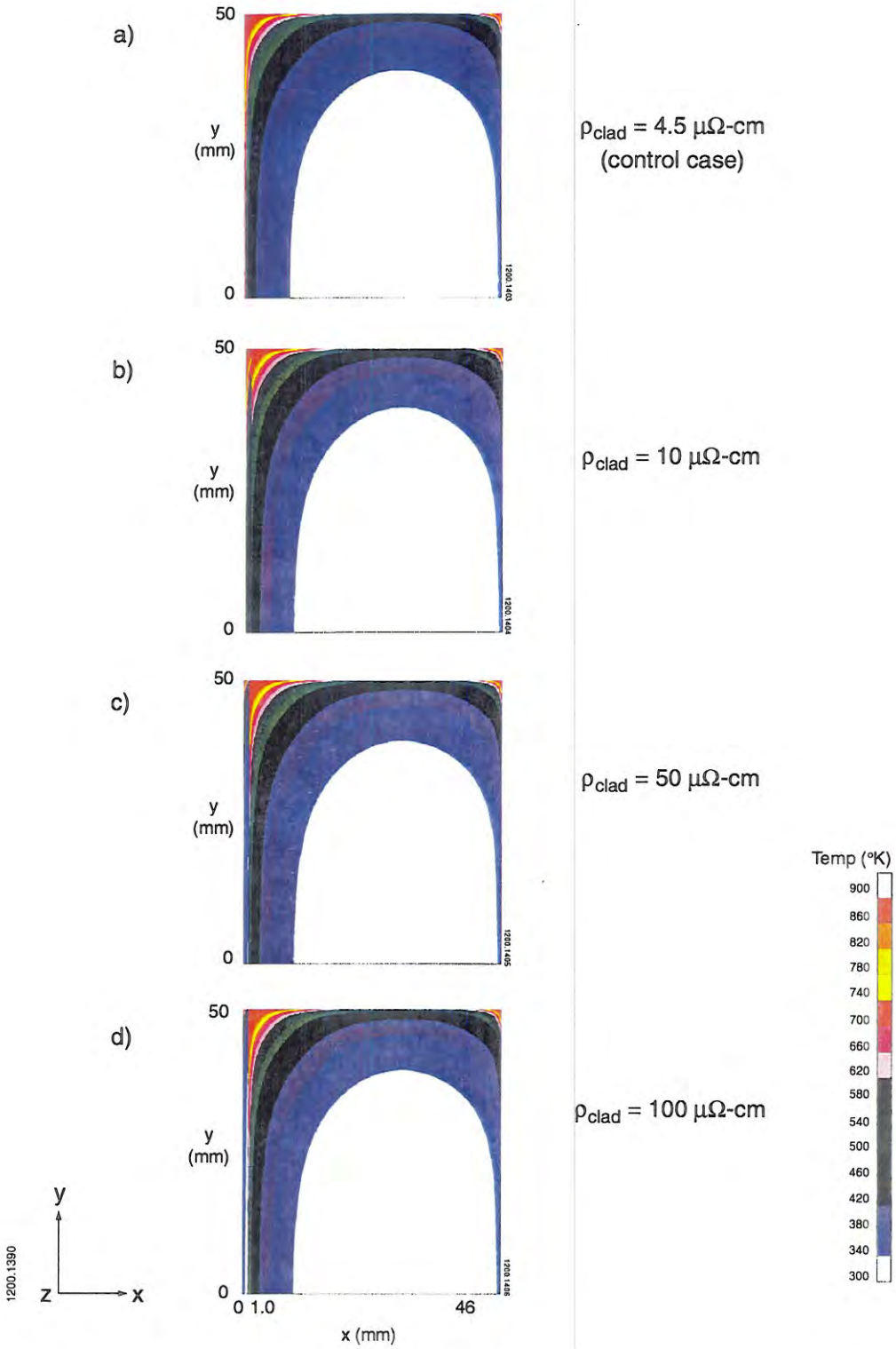

Figure 3. Contour plots of the 2-D EMAP3D calculated temperature distribution of the rail and cladding near the breech at exit time (t_e = 4.2 ms) for four cladding resistivities: ρ = a) 4.5, b) 10, c) 50, d) 100 μΩ•cm.

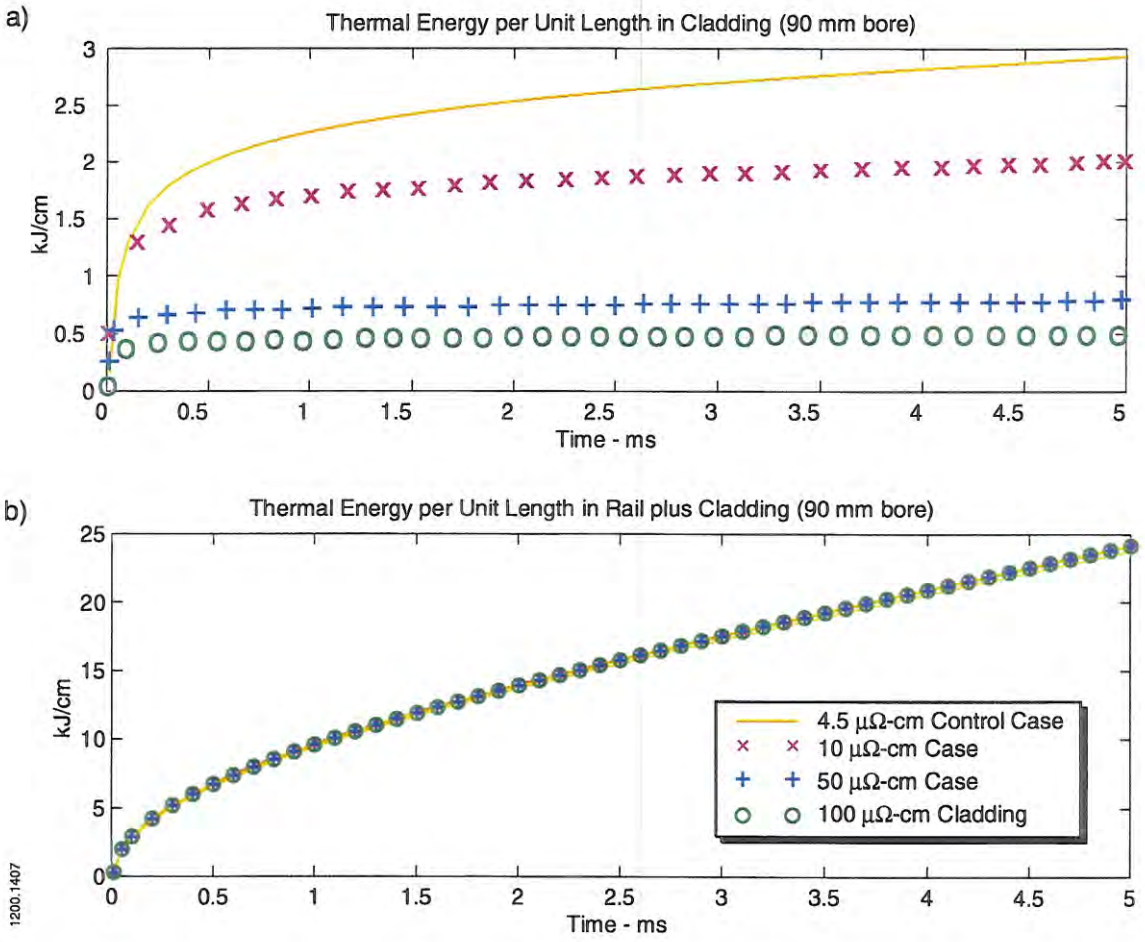

Figure 4. Thermal energy deposited per unit length due to 2-D current diffusion behind the armature. a) Energy gradient in the cladding material. b) Total energy gradient in cladding plus 4.5 μΩ•cm rail.

The total thermal energy deposited during the launch has been calculated assuming a constant acceleration launch [1]: $E_2 = a\int_0^{t_e} E_2'(\tau)\cdot(t_e-\tau)d\tau$. Values for E_2 are tabulated in Table 3.

Table 3. 2D Energy Dissipation for a 4.5 μΩ·cm Rail

Cladding Resistivity ρ (μΩ•cm)	E_2 (MJ)
4.5 (Control)	9.21
10	9.49
50	9.47
100	9.40

For comparison, values of E_2 were calculated for the same claddings assuming a copper rail (ρ = 2 μΩ•cm) rather than the higher resistance rail (ρ = 4.5 μΩ•cm). The corresponding 2D dissipations are given in Table 4. Comparing Tables 3 and 4, there is ~40% reduction in total dissipation, a much larger effect than that due to any of the claddings considered.

Table 4. 2D Energy Dissipation for a 2 μΩ·cm Copper Rail

Cladding Resistivity ρ (μΩ•cm)	E_2 (MJ)
2 (control)	5.60
10	6.32
50	6.18
100	6.10

IV. 3-D Loss Component in Vicinity of Moving Armature

In this section, the additional cladding losses that occur in the vicinity of a moving armature are calculated. These losses are predominantly local to the armature/cladding interface and are governed by the three dimensional nature of the current distribution. In calculations for a 40 mm bore launcher [1], we determined that accurate three dimensional EMAP3D calculations require an impractically fine mesh at large ratios of armature velocity to cladding resistivity, v/ρ. In order to cover the full range of velocity present in a typical launch, analytic formulas for the power dissipation per unit length were derived that have the correct dependence at very large and very small values of v/ρ. EMAP3D calculations were then used to determine the coefficients that provide a smooth connection at intermediate values.

The same procedure has been used for the near full-scale calculation of energy loss in the vicinity of the armature-rail contact. A larger FEM (having more than twice the number of elements) is required for the 90 mm launcher. Thus, even fewer individual calculations were performed and greater reliance on the derived formulas was required in this analysis.

The current density and temperature was simulated for the 90 mm launcher for two armature velocities (v=30 and 100 m/s) and three cladding resistivities (ρ = 10, 50, and 100 μΩ•cm). Figure 5 shows a typical contour plot of |J| flowing in a 4.5 μΩ•cm rail and 50 μΩ•cm cladding. The armature velocity is 100 m/s and the time is 0.99 ms after application of the 3.9 MA current. Details of this case will be described before summarizing the results of 3D cladding loss calculations.

Figure 5 illustrates a point that is important to understanding the energy dissipation in a clad rail. The current density in the cladding is very low except for the area directly in contact with the armature. The high resistivity forces the current to flow directly through the cladding into the rail beneath, thus limiting the power dissipation in the cladding.

Figure 6 shows the temperature profile generated by the current flowing through the cladding. Heating occurs predominantly along the edge of the armature contact where high current density is created by velocity skin effect. Note that the temperature is low at the front edge of the armature where current is just beginning to flow. The temperature rises steadily under the armature where current has been flowing for a longer time. Behind the rear edge of the armature the cladding temperature becomes constant because there is no longer any current flow through the cladding.

In contrast, the temperature of the rail corner begins to rise somewhat behind the front of the armature and continues to rise behind the armature. This continuing heating behind the armature is evaluated in the earlier 2D calculations. Note that the very high corner temperatures result from treating the rail resistivity as independent of temperature. The output of the 3D calculation, E_3', is the thermal energy per unit length in the first mesh zone behind the trailing edge of the armature.

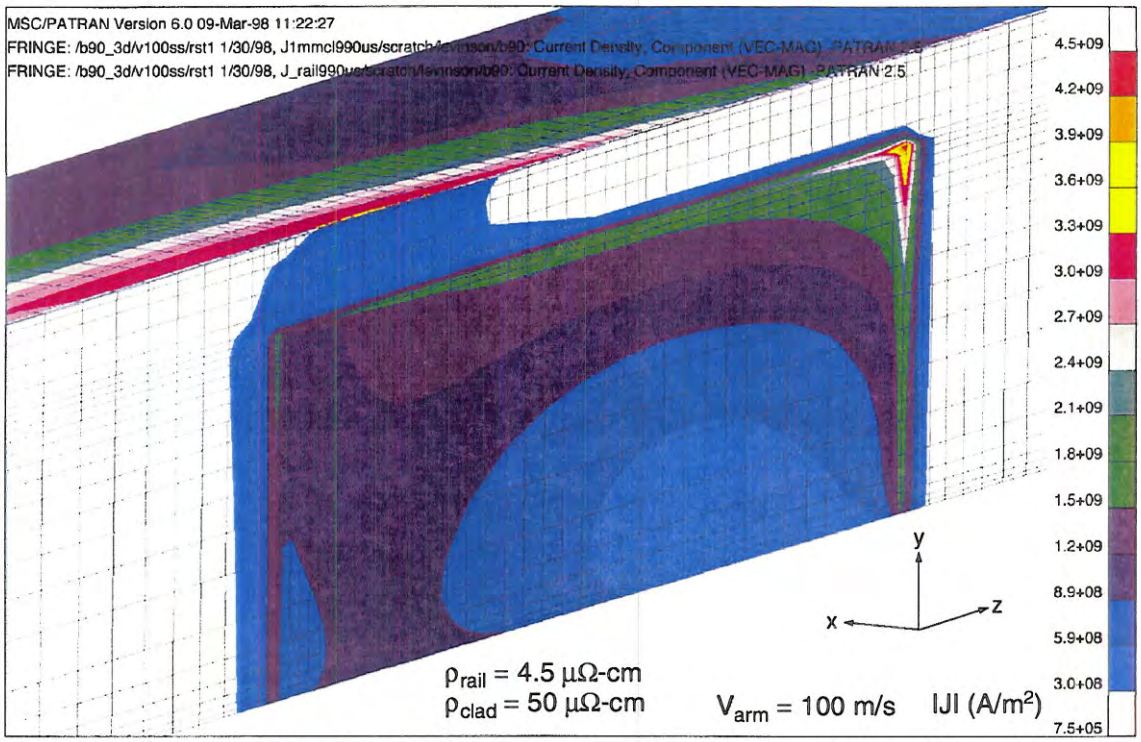

Figure 5. Contour plot of the rail and cladding current distribution |J(x,y,z)| at the armature interface. t=1 ms. 3-D calculation using EMAP3D.

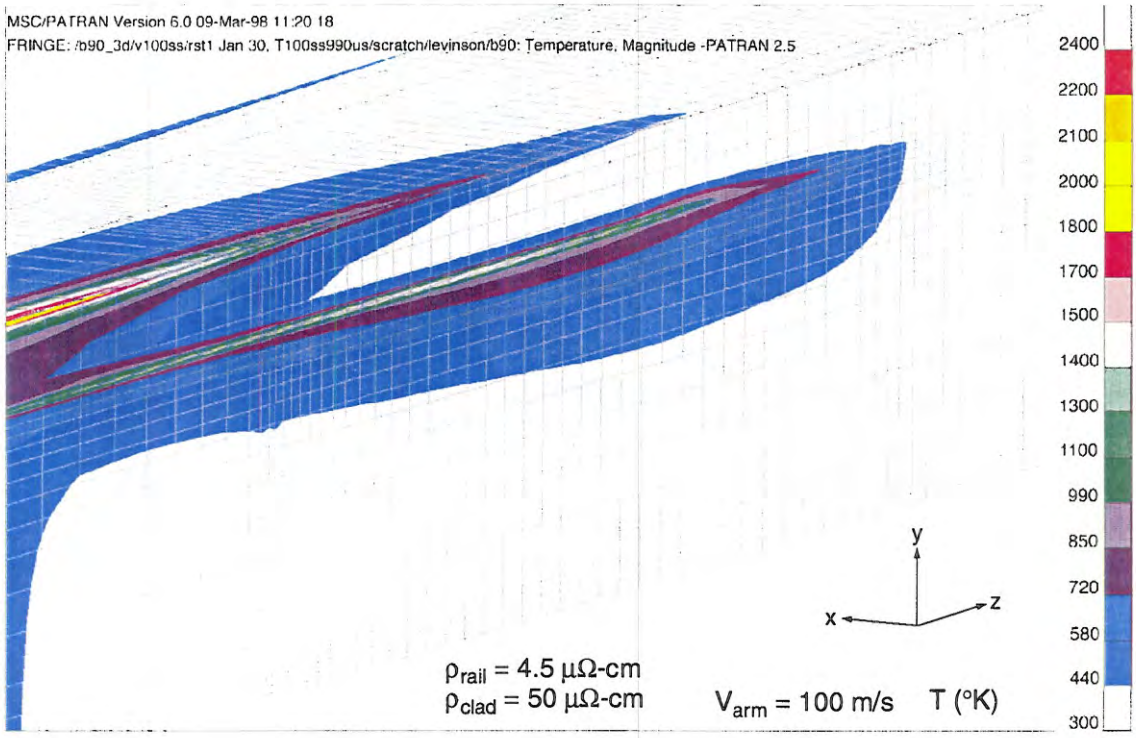

Figure 6. Contour plot of the rail and cladding temperature distribution in the vicinity of the armature. t=1 ms. 3-D calculation using EMAP3D.

In order to calculate E_3' accurately, the armature motion over the rail must be calculated in many small time steps, each of which results in a physical displacement of the armature that is much smaller than its length. It is not practical to use such small steps for the entire launch, so the 3-D calculation is performed in two phases. In phase I, the armature moves in larger time steps. In this phase, current diffusion in the armature is modeled accurately but not the details of the cladding temperature. In phase II the calculational time step is decreased and the details of rail and cladding heating are computed until transients have died out and E_3' has reached an equilibrium value. Fig 7a and b show how this equilibrium is reached. Fig 7a shows E_3' as a function of the armature motion in Phase II. The armature contact is 4.9 cm long, thus the temperature increases for the first few cm of motion. The value of E_3' then decreases slightly with further motion as the current distribution reaches equilibrium. In Fig. 7b the total E_3' in rail and cladding shows the same approach to equilibrium. It is the final equilibrium values that are used in our calculation of total loss and launcher efficiency.

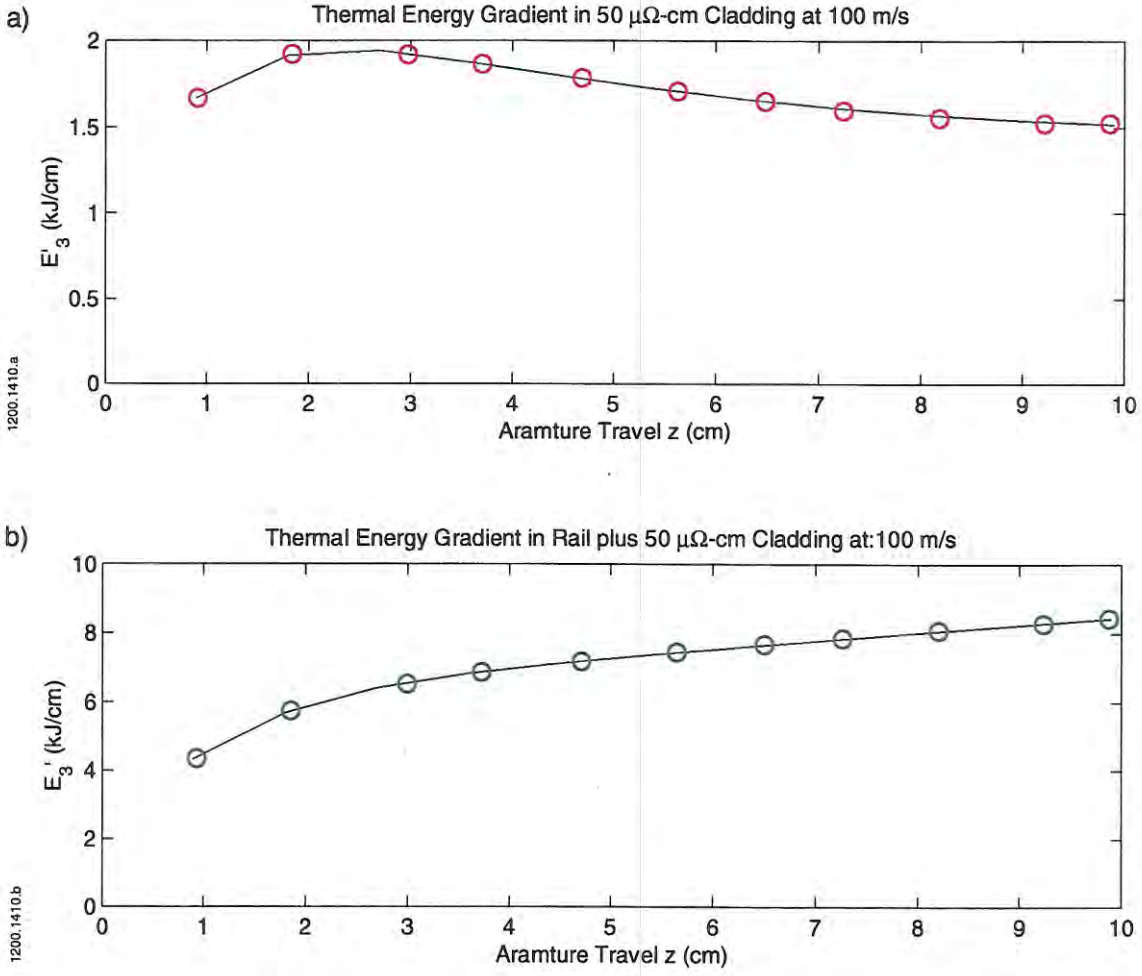

Figure 7. Calculated 3-D component of the thermal energy/unit length as a function of armature motion. The armature must move several times its own length to establish equilibrium. a) Energy gradient in the 50 μΩ•cm cladding only. b) Energy in the 4.5 μΩ•cm rail plus cladding.

Analytic formulas for the energy per unit length dissipated in the cladding, E'_3, were derived in [1]. At low armature velocities (i.e., as $\rho/v \rightarrow \infty$), $E'_3 = E'_{low}(\rho, v) = \frac{2\varepsilon I^2}{A_c}\rho/v$ (refer to Section II of this work for parameter definitions). At high velocities, it was shown that energy per unit length $E'_{high}(\rho, v)$ should scale as $(\rho/v)^{1/2}$. The coefficient of this term cannot be evaluated analytically but can be calculated using an EMAP3D calculation of E'_m at some convenient reference values $\rho=\rho_o$ and $v=v_o$. Then E'_3 at high velocity can be evaluated for arbitrary ρ and v by $E'_3 = E'_{high}(\rho, v) = \frac{E'_m}{(\rho_o / v_o)^{1/2}}(\rho/v)^{1/2}$. The 3-D contribution to total energy deposition can be evaluated by integrating E'_3 over the launcher length using E'_{low} up to some crossover velocity v_c and E'_{high} from v_c to v_e. The resulting formula is $E_3(\rho,v) = \frac{2\varepsilon I^2 \rho v_c}{aA_c} + \frac{2E'_m v_o^{1/2}\rho^{1/2}}{3a\rho_o^{1/2}}\left(v_e^{3/2} - v_c^{3/2}\right)$.

For the near full-scale launcher parameters given in Section II, $E'_{low}(\rho,v)=7.78\cdot10^{12}\rho/v$. The coefficient of $E'_{high}(\rho,v)$, evaluated using EMAP3D calculations at armature velocities 30 and 100 m/s, yields $E'_{high}(\rho,v) = 2.03\cdot10^{9}\ (\rho/v)^{1/2}$ (MKSA units). Fig 8 is a plot of E'_{low} and E'_{high} versus ρ/v along with the EMAP3D calculated points used to derive the coefficient of E'_{high}. Evaluation of the two terms of E_3 for the near full-scale launcher shows that the 3D dissipation resulting from the low velocity term, E'_{low}, is negligible, less than 0.1 % of that due to E'_{high}. A similar result was found in the 40 mm analysis because the crossover velocity v_c is low (less than 20 m/s). The 3D cladding dissipation versus cladding resistivity is given in Table 5.

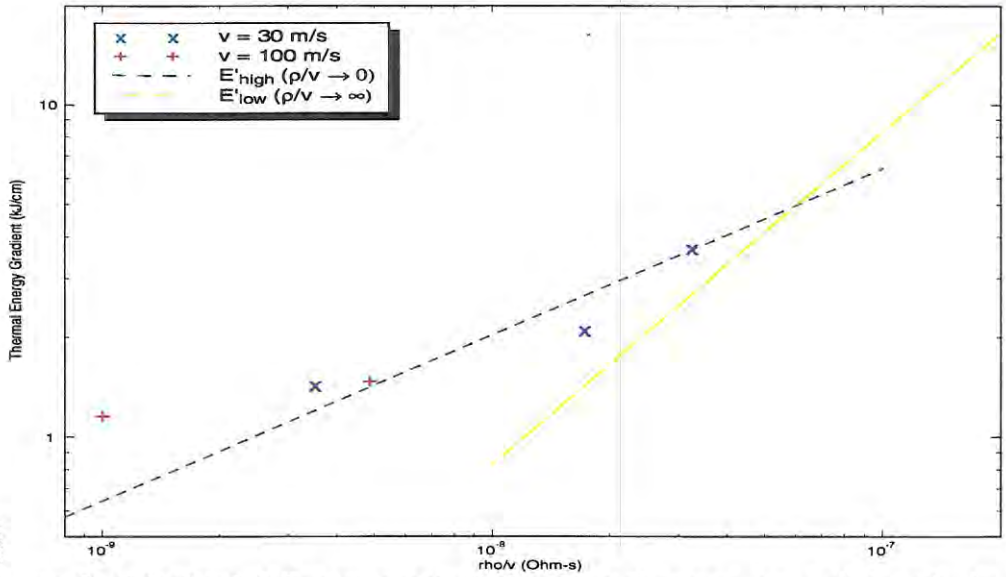

Figure 8. Calculated 3-D component of the thermal energy per unit length in rail plus cladding for 30 and 100 m/s armature velocities. The curve E'_{low} is the theoretical prediction for large ρ/v. The curve E'_{high} has the predicted $\left(\frac{\rho}{V}\right)^{\frac{1}{2}}$ dependence for small ρ/v with a coefficient adjusted to give the best fit to the calculated points.

Table 5. 3D Cladding Dissipation

ρ (μΩ•cm)	E_3(MJ)
10	0.090
50	0.201
100	0.284

Adding together the 2D and 3D contributions, the total dissipation E_{2+3} due to a cladding of various cladding resistivities is given in table 6. The penalty function P for using a resistive cladding, also shown in table 6, is the difference between E_{2+3} with and without the presence of a cladding, divided by the kinetic energy of the launch package at exit.

Table 6. Total Dissipation and Cladding Penalty

ρ (μΩ•cm)	E_{2+3}(MJ)	P (%)
4.5 (Control)	9.21	-
10	9.58	1.81
50	9.67	2.29
100	9.68	2.35

Cladding dissipation has been analyzed in this work only for the single cladding thickness: ε=1 mm. However, current flow through a resistive cladding is essentially one dimensional when ε is much smaller than the largest relevant armature/rail dimension (e.g., ε << any of: W, S, S-W, l_a). Thus, the cladding losses are expected to scale linearly with cladding thickness. The selection of an appropriate cladding thickness for a launcher will require a trade-off between mechanical properties, which favor a thicker cladding, and electrical losses, which favor a thinner cladding.

V. Conclusions

The effect of a 1 mm resistive rail cladding on the electrical losses of a railgun have been investigated numerically in this work for a 90 mm square bore, full-scale launcher with a "C-shaped" aluminum armature. The additional losses due to the 1 mm cladding are less than 2 $^1/_2$ % of the muzzle kinetic energy. This is about 1/2 of the effect calculated for a 40 mm launcher, consistent with our preliminary scaling calculations [2]. The energy dissipation due to two dimensional diffusion was shown to decrease with cladding resistivity, while the dissipation due to 3-D current flow in the vicinity of the armature increases. The total dissipation increases slightly with cladding resistivity. The total energy loss penalty for a 10 μΩ•cm cladding is ΔE_{10} = 9.486-9.214 +0.090 MJ = 362 kJ or 1.81 % of the launch kinetic energy. The 100 μΩ•cm cladding experienced an energy penalty only slightly larger at 2.35 % of the launch kinetic energy.

The effect on overall launcher efficiency is quite small. Without the cladding, the energy input to the launcher at projectile exit is 2 × 20 + 9.21 = 49.21 MJ yielding an overall efficiency (neglecting any recovery of the magnetic energy) of 20/49.21= 0.4064. With the addition of a 100 μΩ•cm cladding, the total energy input increases to 49.68 MJ, and the overall efficiency falls to 0.4026—a decrease of less than 1/2 %. The resistivity of the underlying rail has a much more profound influence on launcher efficiency, and the development of lower resistivity, low density rail materials could easily offset any losses attributable to a resistive cladding.

Acknowledgment

This work was supported by the U.S. Army Research Laboratory (ARL) under contract DAAA21-93-C-0101.

References

[1] Scott Levinson, Jerry Parker, Kuo-Ta Hsieh, and Bok-Ki Kim, "Electrical and Thermal Effects of Rail Cladding," to be presented at 9th EML Symposium, Edinburgh, UK, 1998 and will appear in IEEE Trans. on Magn., Jan, 1999.

[2] Jerry Parker, "Integrated Launch Package Designs - Resistive Cladding," Electric Armaments Review, 22-23-Jan, 1997, Austin TX.

Appendix A

"Electrical and Thermal Effects of Rail Cladding"

Electrical and Thermal Effects of Rail Cladding

Scott Levinson, Jerald V. Parker and Kuo-Ta Hsieh
Institute for Advanced Technology, The University of Texas at Austin, 4030-2 W. Braker Lane, Austin, TX 78759

Bok-ki Kim
Institute for Advanced Technology, The University of Texas at Austin, 4030-2 W. Braker Lane, Austin, TX 78759
Kwangwoon University, 477-1 Wolgye-dong, Nowon-gu, Seoul, Korea

***Abstract*—Achieving long rail life may require the use of a thin surface cladding of hard, refractory material. This paper reports numerical simulations of the effect of a resistive cladding on railgun efficiency. Simulations are performed using a three-dimensional (3-D) finite element code, *E*lectro-*M*echanical *A*nalyses *P*rogram in *3 D*imensions (EMAP3D), that is capable of tracking moving conductors. Current and temperature distributions are calculated in two regions of interest: i) behind the armature—where current diffuses into the rail in a two-dimensional manner, and ii) in the portion of the rail adjacent to and under the armature—where current flow is fully three dimensional. The railgun model used for these simulations has a 40-mm square bore with a 1 mm thick cladding on the rail surface. The increase in electrical loss due to the cladding is a function of axial location and is largest where the armature velocity is low. We find that combined 2-D and 3-D effects cause a total additional thermal loss equal to about 5% of the muzzle energy when the cladding resistivity is 10 or 50 μΩ·cm. The decrease in total launcher efficiency is less than 1%.**

***Index Terms*—cladding, finite element analysis (FEA), loss, railgun.**

I. Introduction

Resistive rail claddings are of interest to the railgun community for several reasons. Claddings with wear properties superior to those of copper offer the potential for increased rail life. In addition, it has been suggested that a thin, resistive layer at the armature/rail interface will neutralize the velocity skin effect by enhancing diffusion, without overheating the rails and armature [1]. A resistive cladding, however, would result in greater overall heating and lower system efficiency.

Manuscript received May 1, 1998.

Scott Levinson, scott_levinson@iat.utexas.edu; Jerry Parker, jerry_parker@iat.utexas.edu; Kuo-Ta Hsieh, kuota_hsieh@iat.utexas.edu; phone: 512-471-9060, fax: 512-471-9096.

This work was supported by the U.S. Army Research Laboratory (ARL) under contract DAAA21-93-0101.

The effects of resistive rails were investigated by Long [2] in a previous work using a two-dimensional finite element code. This work sought to determine whether ohmic heating set a fundamental limit to the velocity of solid armatures—the velocity limit corresponding to the point where any portion of the armature exceeded the melting temperature. A composite rail was modeled consisting of a 1/4-inch section of copper and a 1/4-inch section of molybdenum cladding located on the side adjacent to the armature. It was concluded that, for various armature shapes and materials, the reduction in velocity skin effect due to the resistive cladding was insufficient to compensate for the increased heating at the cladding/armature interface. However, more recent work has shown that two-dimensional analyses are inadequate to describe the current and temperature distributions associated with "C"-type armatures [3].

The objective of this investigation is to reexamine the feasibility of using claddings to improve railgun performance using a 3-D thermal and electromagnetic finite element analysis. We use the code *E*lectro-*M*echanical *A*nalyses *P*rogram in *3 D*imensions (EMAP3D) [4] to compare the electrical losses in a 40-mm square bore launcher with and without resistive rail claddings. The relative importance of cladding loss is quantified using a figure of merit defined as the ohmic losses in the rail cladding divided by the kinetic energy of the launch package at exit.

At present, it is not computationally practical to carry out a 3-D, breech-to-muzzle simulation with the spatial resolution required for this analysis. To overcome this limitation, we compute the resistive losses as the sum of two distinct processes. One process is the diffusion of current into the rail in the region behind the trailing edge of the armature in which ohmic heating is dominated by the axial component of the current in the rail. This calculation is based on a 2-D analysis of diffusion into the rail and cladding. The second process involves losses due to passage of current through the cladding in the vicinity of the armature. A fully 3-D calculation is used to obtain losses in the rail and cladding immediately adjacent to the armature. The 3-D calculations are limited to velocities of 300 m/s or less by the mesh size needed to resolve the thin current layers in the rail. An analytic model of rail cladding heating as a function of resistivity and armature velocity is derived and used to extrapolate the 3-D simulation results to higher armature velocities. Results from both analyses are combined and integrated over the length of the launcher to obtain an

estimate of total ohmic losses in the course of a typical launch.

The paper is organized as follows. Section II describes the finite element model used in the study. In Section III, we describe the results of a 2-D analysis of losses behind the armature. Section IV then treats the 3-D analysis of losses in the cladding in the vicinity of a moving armature. Conclusions based on these analyses are given in Section V.

II. EMAP3D MODEL OF RAIL CLADDINGS

The computer program EMAP3D is the principal tool used for theoretical railgun work at the Institute for Advanced Technology (IAT). It is a 3-D Lagrangian finite element code for solving coupled mechanical, thermal, electromagnetic diffusive processes with moving conductors [4].

In order to facilitate analyses of railgun problems, EMAP3D uses a "reversed motion" mode. In this mode, the armature is stationary, and the rails move backwards past the armature. At each time step, a section of the rail at the breech is removed, and an equal length section is added at the muzzle to maintain the geometry of the analysis domain. This allows the domain to be reduced significantly by limiting the analysis to only the armature and the portion of the rails in the vicinity of the armature. The analysis keeps track of the losses in sections of the mesh that move out of the analysis window at each time step.

Because this is a numerical rather than analytical analysis, it is necessary to choose a particular railgun geometry and typical launch parameters. To facilitate eventual comparison with experiment we have chosen to model the MCL launcher at IAT, a 40-mm square bore device with a rated current of 1.2 MA. The parameters assumed in the calculations are:

- I = 1.0 10^6 (A) constant, total electric current flowing in the launcher
- L' = 0.42 (μH/m) inductive gradient in launcher
- t_e = 2.5 (ms) exit time
- v_e = 2.5 (km/s) exit velocity
- M_a = 210 (g) mass of launch package

which imply:

- F = $L'I^2/2$ = 210 (KN) armature force
- a = 10^6 (m/s^2) constant armature acceleration
- $v(t)$ = 10^6 t (m/s) linear velocity dependence on time t
- $z(t)$ = $5 \cdot 10^5$ t^2 (m) parabolic axial position dependence on time t
- L_0 = 3.125 (m) launcher length
- KE = 0.656 (MJ) muzzle kinetic energy

The symmetries of a railgun/armature system allow it to be completely characterized by modeling only one-quarter of the geometry. Fig. 1 shows the model of armature, rail and claddings used in this investigation. The model consists of the upper half of one rail and the upper quarter of the armature. Fig. 1 also shows the mesh in the FE model of the conductors. Eight-node, linear, brick elements are used for each material. There are a total of 26,334 elements in the mesh. A higher mesh density is used in regions of the conductor where there are high gradients in current density and temperature. The scalar magnetic potential is used in the nonconducting air region of the railgun model (not shown, but extending to X = 0.5 m and Y = 0.5 m) to reduce the large storage and computational times needed to model three-dimensional vector electromagnetic fields [5].

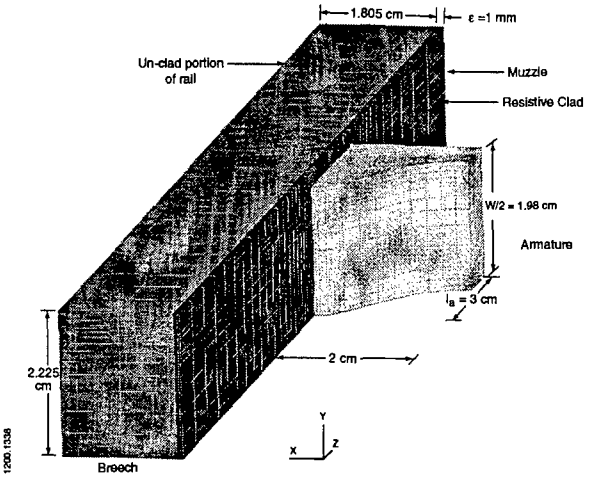

Fig. 1. One-quarter model of railgun geometry and FE mesh.

Some of the material properties used in the model are shown in Fig. 2. The aluminum armature is modeled with constant specific heat and resistivity. The rail is modeled as ETP copper with appropriate temperature-dependent specific heat. The resistivity of the copper, however, has been fixed at 2 $\mu\Omega \cdot$cm (control cladding) to facilitate comparisons with the fixed resistivity cladding. Two fixed cladding resistivities are treated, ρ = 10 and 50 $\mu\Omega \cdot$cm. The specific heat of the cladding is set to that of the copper rail for convenience. The thermal diffusivity of the conductor materials is typically 2-3 orders of magnitude smaller than the magnetic diffusivity [6] and there is little flow of thermal energy during the launch. Accordingly, thermal conduction is turned off in this analysis.

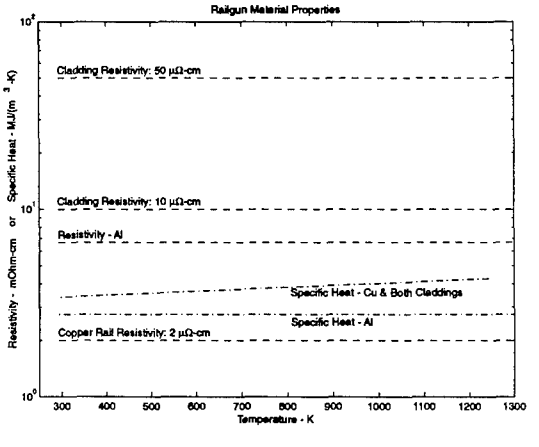

Fig. 2. Railgun material properties.

III. LOSSES AT LARGE DISTANCES FROM THE ARMATURE

In this section, we consider electrical losses in the rail in the region behind the armature. This component of the energy loss is effectively two-dimensional once the armature has moved far enough from a given position that the current density in the rail and cladding is essentially ($\mathbf{J} = J_z$), unaffected by the armature. Thus, the ohmic losses can be obtained from a 2-D calculation of a 1-MA current flowing axially in the rail and cladding without armature. The total energy loss from this term is obtained by integrating over the length of the rail with a local heating rate given by the 2-D solution at a time equal to the time since the armature passed that location.

Fig. 3 summarizes the results of the 2-D analyses. The plots show energy dissipated per unit axial length of rail in both rails as a function of time. Fig. 3a shows energy/unit length dissipated in the individual claddings. All of the materials dissipate significant energy at early time. Energy loss continues in the 2-μΩ·cm cladding (control case), since it continues to carry its share of the rail current throughout the launch. After 100 to 300 μs, however, the cladding does not carry current, and little further heating occurs. Fig. 3b shows the total energy dissipated per unit length in both copper rail and cladding. This quantity, designated E_2', is greater for resistive claddings, as expected.

The effect of current diffusion on heating can be seen in Fig. 4 where the final temperature of the rail and cladding near the breech is shown for three cladding resistivities. The high resistivity cladding is substantially cooler than the underlying copper rail at the end of the launch.

The thermal energy dissipated over the launch can be estimated by integrating the energy gradient over the length of the rail: $E_2 = \int_0^{L_0} E_2'(z)dz$. The required change of variables is made by noting that the dwell time, t, during which current is present at any given axial point in the rail and cladding, is given by $\tau = t_e - t$, where t_e is the time of muzzle exit and t is the time at which the armature reaches point z. Substituting the expression for τ into the acceleration profile $z(t) = 1/2at^2$, the assumed constant acceleration launch condition, allows one to change variable from position to time and to calculate: $E_2 = a\int_0^{t_e} E_2'(\tau)\cdot(t_e - \tau)\cdot d\tau$.

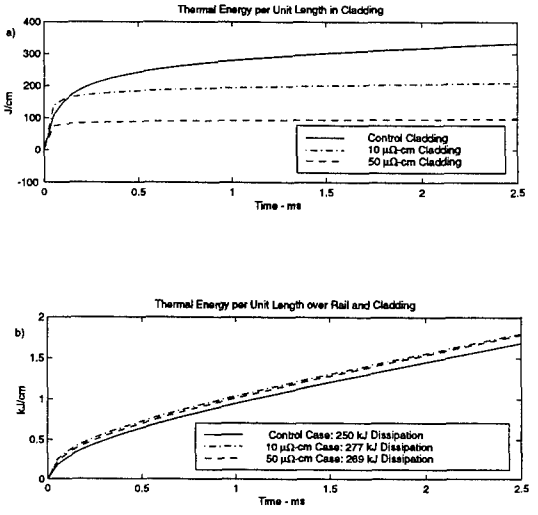

Fig. 3. Thermal energy dissipation per unit length due to 2-D diffusion behind the armature. a) Energy in the cladding materials. b) Energy in cladding and copper rail. The total energy dissipated over the launch is tabulated in the legend.

Values for E_2 are tabulated in the legend of Fig. 3b. The penalty for using a resistive cladding can be written as the difference between E_2 with and without the presence of a cladding, normalized by the kinetic energy of the armature at exit. The resulting penalty $p_2 = \frac{E_{2clad} - E_{2unclad}}{KE}$ is 4.1% for the 10-μΩ·cm cladding and 2.9% for the 50-μΩ·cm cladding.

IV. 3-D CLADDING EFFECTS IN VICINITY OF A MOVING ARMATURE

We now consider energy losses in the cladding in the vicinity of the moving armature. Because accurate EMAP3D calculations of cladding loss require an impractically fine

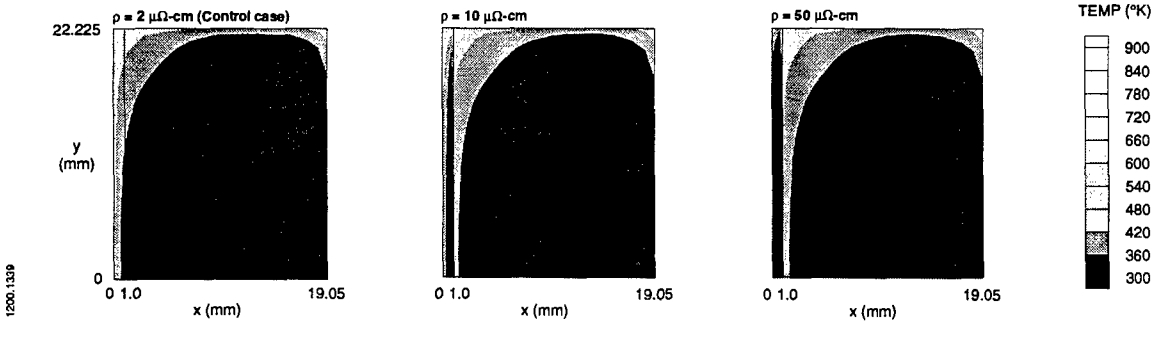

Fig. 4. Contour plots of 2-D EMAP3D calculation of the rail temperature near the breech at exit time (t_e = 2.50 ms) for three cladding resistivities: ρ = 2, 10, 50 μΩ·cm. The peak temperature (1070 K) for the 2 μΩ·cm cladding (control case) occurs at the inner corner of the cladding; lower temperature peaks (less than 900 K) exist in both the cladding and copper sections of the rail for both resistive claddings.

mesh when the ratio of armature velocity to cladding resistivity v/ρ is greater than $\sim \frac{100 \cdot m/s}{10 \cdot \mu\Omega \cdot cm}$, our strategy is to derive asymptotic formulas that bound resistive cladding losses at the velocity extremes and use accurate EMAP3D calculations at intermediate velocities (30 and 100 m/s). We then obtain the losses over the launch by computing the energy dissipation per unit length (designated E_3') in a region immediately behind the armature, and integrating it over the launch.

The formulas derived to bound resistive cladding losses are based on the assumption that the cladding resistivity is several times greater than the resistivity of either the armature or the unclad portion of the rail. At extremely low armature velocities, current will flow uniformly from the unclad rail through the cladding and into the armature. In this regime, the cladding losses can be calculated using Ohm's law. At extremely high armature velocities, cladding losses will be confined to a thin diffusion layer on the cladding surface due to velocity skin effect.

A. Cladding Loss Gradient for Low Armature Velocity

At extremely low armature velocities, an almost uniform current density exists in the cladding given by $j = I/w\ell_a$, where I is the total current through the armature, and w and ℓ_a are armature dimensions identified in Fig. 1. The resulting thermal energy density dissipated in the cladding as the armature moves across it at velocity v may be expressed in terms of a product of the heating rate density ρj^2 in the cladding and the time of contact $\Delta t = \frac{\ell_a}{v}$ with the armature: $\frac{Energy}{vol} = \frac{\rho \cdot I^2}{w^2 \ell_a v}$. Therefore, the thermal energy per unit length for claddings of thickness ε on both rails due to armature passage at low velocities is:

$$E'_{low}(\rho,v) = \frac{2Energy}{vol} w\varepsilon = \frac{2\varepsilon I^2}{w\ell_a}\frac{\rho}{v} = 1.66*10^{12}\frac{\rho}{v} \text{ (in J/m).} \quad (1)$$

The value E'_{low} is a minimum value of E_3'. Any process that makes the current distribution less uniform will increase E_3'. For example, if the current flows only in the outer half of the cladding, the energy gradient doubles.

B. Cladding Loss Gradient for High Armature Velocity

In the high velocity regime current penetration into the rail near the armature is small and, to a good approximation, the current density may be written as: $j(x,y,z,t) = \frac{J_s(\ell,z)}{\delta(\ell,z(t))}$, where $J_s(\ell,z)$ is the surface current density, ℓ is a generalized coordinate on the surface that is perpendicular to the motion, z is a coordinate parallel to the motion, and δ is the diffusion depth at point (ℓ,z) in the cladding. To obtain the energy deposited/unit length E'_{high} for high armature velocities, we pick a point on the rail and integrate the heating rate ρj^2 over transverse coordinate ℓ and over the time duration corresponding to armature passage, replacing the integral over depth with the diffusion depth:

$$E'_{high} = \iint \frac{\rho J_s^2(\ell,z)}{\delta^2(\ell,z(t))}\delta(\ell,z)d\ell dt.$$

A velocity-dependent diffusion depth $\delta = \delta_v$ is implicitly a function of the time and requires 3-D simulation to obtain accurately. Once $\delta_{v_0}(\ell,z(t))$ is known at a particular velocity v_0 and cladding resistivity ρ_0, however, it is a good approximation that $\delta_v(\ell,z) = \delta_{v_0}(\ell,z)\sqrt{\frac{v_0}{\rho_0}}\sqrt{\frac{\rho}{v}}$, because diffusion into the cladding is essentially one dimensional at high velocity. Using this relation and replacing the integral over time by an integral over z using $z = vt$, the expression for E'_{high} becomes:

$$E'_{high}(\rho,v) = \iint \frac{\rho J_s^2(\ell,z)}{\sqrt{\frac{v_0\rho}{v\rho_0}}\delta_{v_0}(\ell,z)} d\ell \frac{dz}{v} =$$

$$\sqrt{\frac{\rho v_0}{\rho_0 v}} \iint \frac{\rho_0 J_s^2(\ell,z)}{\delta_{v_0}(\ell,z)v_0} d\ell dz = E'_m \sqrt{\frac{v_0}{\rho_0}}\sqrt{\frac{\rho}{v}}. \quad (2)$$

Equation 2 provides a convenient scaling relationship that can be used to extend E′ to higher velocity once an accurate value of E'_m is known at some reference velocity v_0 and cladding resistivity ρ_0.

C. Simulated Cladding Losses with Armature Motion

Energy dissipation in the cladding was calculated at velocities 30 and 100 m/s using EMAP3D. In order to verify the scaling relationships, (1) and (2), calculations were performed for five resistivities spanning the range 10 to 200 μΩ·cm. For each calculation, a series of time steps was taken at constant velocity until the armature had moved 50 mm (1.7 times the contact length). At this point, the energy deposition in the cladding had reached equilibrium, and the energy gradient E'_m was evaluated in a 0.6 mm long region located 0.4 mm behind the trailing edge of the armature.

Fig. 5 summarizes the results obtained from the 3-D analyses. The calculated values are plotted with "x" for the 30 m/s results and "+" for the 100 m/s results. The dot-dash line is a plot of $E'_{low}(\rho,v)$. There is excellent agreement between the EMAP3D and the analytic theory in the limit of high resistivity. The dashed line represents the scaling relationship (2). The unknown coefficient $E'_m\sqrt{v_0/\rho_0}$ has been adjusted to fit the EMAP3D calculation at $\rho_0 = 20$ μΩ·cm, $v_0 = 30$ m/s. The agreement between

calculation and theory is less satisfactory at small ρ/v, and in fact, the calculated energy begins to rise as ρ/v decreases below 10^{-9} Ω–s. Such behavior is clearly incorrect, since the dissipation must approach zero in the limit of zero resistivity. This behavior is attributable to a progressive inaccuracy in the calculation for small ρ/v as the diffusion depth due to velocity skin effect becomes small compared to the mesh resolution. The final expression adapted for our analyses,

$$E'_{high}(\rho,v) = 2.06\cdot 10^{8}\left(\frac{\rho}{v}\right)^{\frac{1}{2}}, \quad \text{(MKS units)} \qquad (3)$$

is conservative in that it generally has values above those calculated at 100 m/s, and probably overpredicts the actual losses.

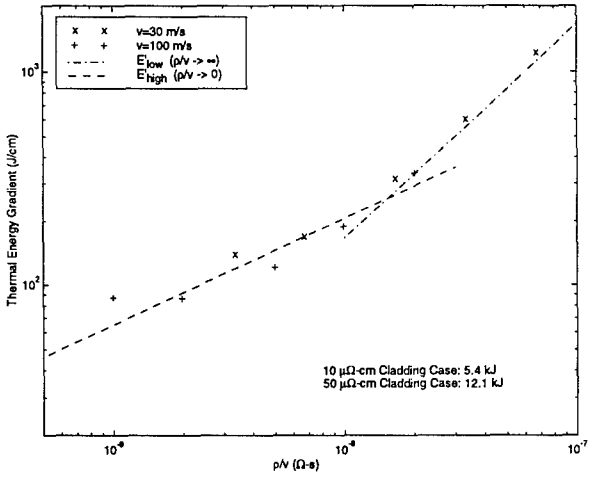

Fig. 5. Calculated thermal energy per unit length in rail and cladding for 30 and 100 m/s armature velocities. Symbols indicate estimates of E'_3 determined from EMAP3D calculations. Curves E'_{low} and E'_{high} are asymptotes for extreme values of ρ/v. Upper bounds for thermal dissipation due to armature passage are shown in the lower legend.

In order to complete the calculation of total energy dissipation, the two expressions for E'_3 given by (1) and (3) must be integrated over the length of the launcher. Equation 1 is used in the beginning of the launch, changing to (3) at the crossover velocity $v_c = 6.67\cdot 10^{7}\rho$.

Using the relationship $z = v^2/2a$ (for a constant acceleration launch) to change variables from position to velocity, the total energy dissipated due to 3-D effects near the armature becomes

$$E_3 = \frac{1}{a}\left(1.66\cdot 10^{12}\rho\cdot v_c + 1.373\cdot 10^{8}\sqrt{\rho\cdot\left(v_e^3 - v_c^3\right)}\right). \quad \text{(MKS units)} \qquad (4)$$

Because the crossover velocity v_c is low for the resistivities of interest, the first term in (4) contributes less than 1% to E_3. The calculated values of E_3 for a 40-mm launcher using (4) are 5.4 kJ and 12.1 kJ for 10-μΩ·cm and 50-μΩ·cm cladding resistivities, respectively. The 3-D resistive cladding penalty $p_3 = \frac{E_3}{KE}$ is 0.82% for the 10-μΩ·cm cladding and 1.85% for the 50-μΩ·cm cladding.

V. Conclusions

The effects of a 1-mm resistive rail cladding on the electrical losses of a railgun have been investigated numerically in this work for a 40-mm square bore launcher with a "C"-shaped aluminum armature. The calculations were divided into two parts, a 2-D diffusion calculation for the rail behind the armature and a 3-D moving armature calculation of energy dissipation in the vicinity of the armature.

Far behind the armature, energy dissipation in the rails due to 2-D diffusion through the cladding exhibits a peak in dissipation as a function of cladding resistivity. At low resistivity, the cladding shares the current during the entire launch. The reduced current density results in lower dissipation. At very high resistivity, 2-D diffusion through the cladding is essentially instantaneous, resulting in little energy dissipation in the cladding and a somewhat increased dissipation in the underlying rail due to its reduced area. At intermediate resistivity, there is significant dissipation in the cladding leading to a higher overall energy dissipation during the 2-D diffusion through the cladding. For our 2-D analysis, the intermediate cladding resistivity (ρ = 10 μΩ·cm) resulted in higher overall losses (277 kJ) than either the control case (ρ = 2 μΩ·cm with 250 kJ) or the high resistivity case (ρ = 50 μΩ·cm with 269 kJ). We also observe that the peak rail and cladding temperatures are lower in rails having resistive claddings.

Energy dissipation in the claddings due to the 3-D current flow around the armature is smaller in magnitude than the 2-D energy loss and exhibits a continuous increase proportional to $\rho^{0.5}$. Therefore variations arising from differences in armature designs should not significantly affect overall launcher efficiency when a cladding is used. The total energy loss penalty for the 10-μΩ·cm cladding is ΔE_{10} = 277 - 250 + 5.4 = 32.4 kJ or 4.9% of the launch kinetic energy. For the 50-μΩ·cm cladding, the energy penalty is nearly identical, ΔE_{50} = 269-250 +12.1 = 31.1 kJ or 4.7% of the launch kinetic energy. The effect on overall launcher efficiency is quite small. Without the cladding, the energy input to the launcher at projectile exit is 2 × 656 + 250 = 1562 kJ yielding an overall efficiency (neglecting any recovery of the magnetic energy) of 656/1562 = 0.42. With the addition of a 10-μΩ·cm cladding, the total energy input increases to 1594 kJ, and the overall efficiency falls to 0.411—a decrease of less than 1%.

Acknowledgment

The authors wish to thank Francis Stefani for numerous critical discussions reflected in this work. The authors wish to acknowledge computational support from the High Performance Computing Facility, The University of Texas at Austin.

REFERENCES

[1] Y. A. Driezen, "Solid armature performance with resistive rails" *IEEE Trans. Magn.*, 29, pp. 798-803, January 1993.

[2] G. C. Long, *Fundamental Limits to the Velocity of Solid Armatures in Railguns*, Ph.D. Dissertation, The University of Texas at Austin, Publication Number TD-35, August 1987.

[3] J. D. Powell and A. E. Zielinski, "Current and Heat Transport in the Cannon-Caliber Electromagnetic Gun Armature," Army Research Laboratory, ARL-MR-258, August 1995.

[4] K. T. Hsieh, "A Lagrangian formulation for mechanically, thermally coupled electromagnetic diffusive processes with moving conductors," *IEEE Trans. Magn.*, vol. 31, pp. 605-609, January 1995.

[5] K. T. Hsieh and B. K. Kim, "Implementing tri-potential approach in EMAP3D," to be presented at the 9th EML Symposium, Edinburgh, UK, 1998.

[6] *Pulsed High Magnetic Fields*, H. Knoepfel, London: North Holland Publishing Co., 1970.

Distribution List

Administrator
Defense Technical Information Center
Attn: DTIC-DDA
8725 John J. Kingman Road,
Ste 0944
Ft. Belvoir, VA 22060-6218

Director
US Army Research Lab
ATTN: AMSRL OP SD TA
2800 Powder Mill Road
Adelphi, MD 20783-1145

Director
US Army Research Lab
ATTN: AMSRL OP SD TL
2800 Powder Mill Road
Adelphi, MD 20783-1145

Director
US Army Research Lab
ATTN: AMSRL OP SD TP
2800 Powder Mill Road
Adelphi, MD 20783-1145

Army Research Laboratory
AMSRL-CI-LP
Technical Library 305
Aberdeen Prvg Grd, MD 21005-5066

Mr. Dave Bauer
IAP Research, Incorporated
2763 Culver Avenue
Dayton, OH 45429-3723

Dr. Bruce Burns
U.S Army Research Laboratory
Attn: AMSRL-WT-PD
Bldg. 390
Aberdeen Prvg Grd, MD 21005-5066

Dr. George Chryssomallis
Science Applications International Corp.
3800 W. 80th St., Suite 1090
Bloomington, MN 55431

Mr. Dan Dakin
Science Applications International Corp.
2000 Powell St., Suite 1090
Emeryville, CA 94608

Dr. Harry Fair
Institute for Advanced Technology
The University of Texas at Austin
4030-2 West Braker Lane
Austin, TX 78759

Dr. Scott Fish
Institute for Advanced Technology
The University of Texas at Austin
4030-2 W. Braker Lane
Austin, TX 78759

Ms. Rachel Gee
Institute for Advanced Technology
The University of Texas at Austin
4030-2 W. Braker Lane
Austin, TX 78759

Dr. Thaddeus Gora
U.S. Army Armament Research,
Development and Engineering Center
Attn: AMSTA-AR-FS Bldg. 94
Picatinny Arsenal, NJ 07806-5000

Dr. Robert Guenther
Army Research Office
P.O. Box 12211
Research Triangle Park, NC 27709-2211

Mr. Albert Horst
Chief, Propulsion and Flight Division
Army Research Laboratory
ATTN: AMSRL -WT-P
Army Research Laboratory
Aberdeen Prvg Grd, MD 20115-5066

Dr. Kuo-Ta Hsieh
Institute for Advanced Technology
The University of Texas at Austin
4030-2 W. Braker Lane
Austin, TX 78759

Dr. Keith A. Jamison
Science Applications International Corp.
1247-B N. Eglin Parkway
P. O. Box 126
Shalimar, FL 32579

Dr. Walter LaBerge
Institute for Advanced Technology
The University of Texas at Austin
4030-2 West Braker Lane
Austin, TX 78759

Mr. Dennis Ladd
COMMANDER, TACOM-ARDEC
ATTN: AMSTA-AR-FSP-E / Dennis Ladd
Bldg. 354
Picatinny Arsenal, NJ 07806-5000

Dr. Scott Levinson
Institute for Advanced Technology
The University of Texas at Austin
4030-2 W. Braker Lane
Austin, TX 78759

Dr. Hans Mark
Institute for Advanced Technology
The University of Texas at Austin
4030-2 West Braker Lane
Austin, TX 78759

Distribution List

Dr. Ingo W. May
Office of the Director
Army Research Laboratory
ATTN: AMSRL -WT
Army Research Laboratory
Aberdeen Prvg Grd, MD 20115-5066

Dr. Edward M. Schmidt
U.S. Army Research Laboratory
Attn: AMSRL-WT-B
Aberdeen Prvg Grd, MD 21005-5066

Dr. Ian McNab
Institute for Advanced Technology
The University of Texas at Austin
4030-2 W. Braker Lane
Austin, TX 78759

Mr. Francis Stefani
Institute for Advanced Technology
The University of Texas at Austin
4030-2 W. Braker Ln.
Austin, TX 78759

Dr. Jerry Parker
Institute for Advanced Technology
The University of Texas at Austin
4030-2 W. Braker Lane
Austin, TX 78759

Mr. Patrick Sullivan
Institute for Advanced Technology
The University of Texas at Austin
4030-2 West Braker Lane
Austin, TX 78759

Dr. John Parmentola
Office of the Assistant Secretary
of the Army (RDA)
Deputy Asst. Secretary of the
Army for Research & Technology
The Pentagon, Room 3E374
Washington, DC 20310-0103

Mr. Robert J. Taylor
Lockheed Martin Vought Systems
M/S: WT-21
P.O. Box 650003
Dallas, TX 75265-0003

Dr. Chadee Persad
Institute for Advanced Technology
The University of Texas at Austin
4030-2 W. Braker Lane
Austin, TX 78759

Mr. Alex Zielinski
U.S. Army Research Laboratory
AMSRL-WT-PB, B390, RM 212
Aberdeen Prvg Grd, MD 21005-5066

Dr. John Powell
U.S Army Research Laboratory
Attn: AMSRL-WT-WD
Bldg. 120
Aberdeen Prvg Grd, MD 21005-5066

Mr. Raymond C. Zowarka
Center for Electromechanics
The University of Texas at Austin
Pickle Research Campus
EME 13, C R 7000
Austin, TX 78712

Mr. Bob Schlenner
U.S. Army Armament Research,
Development and Engineering Center
Attn: AMSTA-AR-CCL
Bldg. 65N
Picatinny Arsenal, NJ 07806-5000